17. M. G. Ramsey, D. Steinmüller, M. Schatzmayr, M. Kiskinova, F. P. Netzer, *Chem. Phys.* **177**, 349 (1993).
18. J. P. Maier, D. W. Turner, *Faraday Discuss. Chem. Soc.* **54**, 149 (1972).
19. R. Hoffmann, *Solids and Surfaces: A Chemist's View of Bonding in Extended Structures* (Wiley-VCH, New York, 1988).
20. J. Ivanco, B. Winter, F. P. Netzer, M. G. Ramsey, *Adv. Mater.* **15**, 1812 (2003).
21. B. Winter *et al.*, *Appl. Phys. Lett.* **88**, 253111 (2006).
22. E. L. Shirley, L. J. Terminello, S. Santoni, F. J. Himpsel, *Phys. Rev. B* **51**, 13614 (1995).
23. D. Yoshimura *et al.*, *J. Chem. Phys.* **120**, 10753 (2004).
24. Whereas structural studies have concluded that 6P is "on average planar" in the solid state, our measurements on numerous films on a variety of substrates always yield the ionization potential (IP) of the twisted conformation when the molecules are oriented parallel to the substrate. In contrast, films of upright molecules [6P(001)] yield a higher IP, in keeping with a planar conformation. The observed twist, we believe, is the result of a novel surface reconstruction of these molecular crystals, lowering the total energy.
25. This work was supported by the Austrian Science Funds (FWF).

Supporting Online Material
www.sciencemag.org/cgi/content/full/317/5836/351/DC1
Materials and Methods
Figs. S1 to S5
References

30 March 2007; accepted 5 June 2007
10.1126/science.1143239

Spontaneous Superlattice Formation in Nanorods Through Partial Cation Exchange

Richard D. Robinson,[1] Bryce Sadtler,[2]* Denis O. Demchenko,[3]* Can K. Erdonmez,[2] Lin-Wang Wang,[3] A. Paul Alivisatos[1,2]†

Lattice-mismatch strains are widely known to control nanoscale pattern formation in heteroepitaxy, but such effects have not been exploited in colloidal nanocrystal growth. We demonstrate a colloidal route to synthesizing CdS-Ag_2S nanorod superlattices through partial cation exchange. Strain induces the spontaneous formation of periodic structures. Ab initio calculations of the interfacial energy and modeling of strain energies show that these forces drive the self-organization of the superlattices. The nanorod superlattices exhibit high stability against ripening and phase mixing. These materials are tunable near-infrared emitters with potential applications as nanometer-scale optoelectronic devices.

The ability to pattern on the nanoscale has led to a wide range of advanced artificial materials with controllable quantum energy levels. Structures such as quantum-dot arrays and nanowire heterostructures can be fabricated by vacuum- and vapor-deposition techniques such as molecular beam epitaxy (MBE) and vapor-liquid-solid (VLS) processes, resulting in quantum-confined units that are attached to a substrate or embedded in a solid medium (*1*–*5*). A target of colloidal nanocrystal research is to create these same structures while leveraging the advantages of solution-phase fabrication, such as low-cost synthesis and compatibility in disparate environments [e.g., for use in biological labeling (*6*, *7*) and solution-processed light-emitting diodes (*8*) and solar cells (*9*)]. One key difference between quantum dots epitaxially grown on a substrate and free-standing colloidal quantum dots is the presence of strain. In epitaxially grown systems, the interface between the substrate crystal and the quantum dot creates a region of strain surrounding the dot. Ingeniously, this local strain has been used to create an energy of interaction between closely spaced dots; this use of "strain engineering" has led, in turn, to quantum-dot arrays that are spatially patterned in two (and even three) dimensions (*2*–*4*). We demonstrate the application of strain engineering in a colloidal quantum-dot system by introducing a method that spontaneously creates a regularly spaced arrangement of quantum dots within a colloidal quantum rod.

A linear array of quantum dots within a nanorod effectively creates a one-dimensional (1D)

[1]Materials Science Division, Lawrence Berkeley National Laboratory, Berkeley, CA 94720, USA. [2]Department of Chemistry, University of California, Berkeley, CA 94720, USA. [3]Computational Research Division, Lawrence Berkeley National Laboratory, Berkeley, CA 94720, USA.
*These authors contributed equally to this work.
†To whom correspondence should be addressed. E-mail: alivis@berkeley.edu

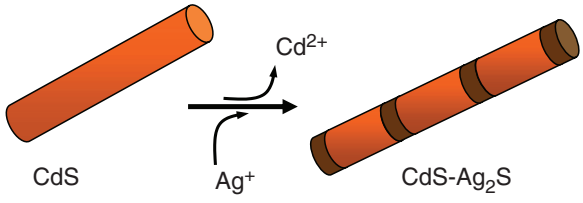

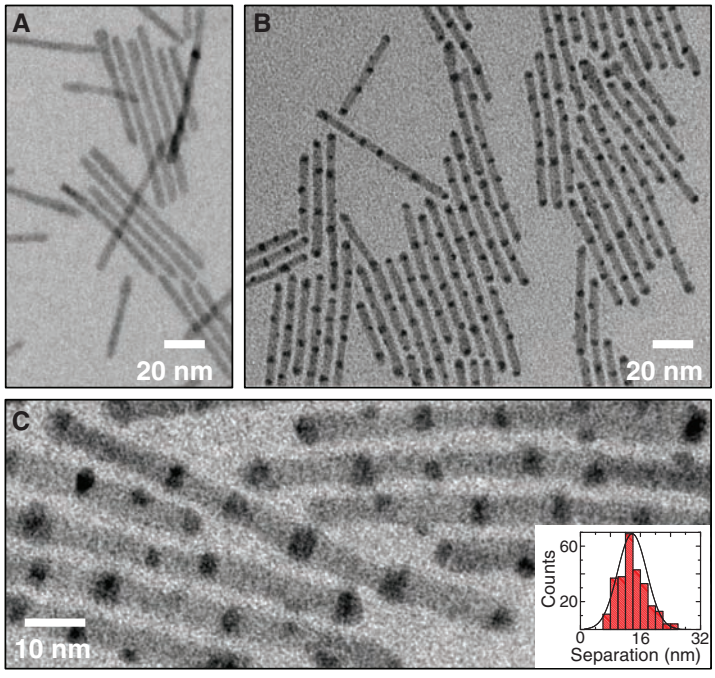

Fig. 1. TEM images of superlattices formed through partial cation exchange. (**A**) The original 4.8–by–64-nm CdS nanorods. (**B** and **C**) Transformed CdS-Ag_2S superlattices. (Inset) Histogram of Ag_2S segment spacing (center-to-center). The average spacing is 13.8 ± 3.8 nm. The sample set for the histogram was greater than 250 spacings.

superlattice, a promising new generation of materials (*10*, *11*). Such 1D superlattices exhibit confinement effects and are unusual because of their ability to tolerate large amounts of lattice mismatch without forming dislocations and degrading device performance (*12*, *13*). Strong coupling of electronic states makes them interesting for optical systems and good candidates for photonic applications. One-dimensional superlattices are also of interest for thermoelectric devices and the study of ionic transport in 1D systems. VLS growth has demonstrated the formation of extended nanowire superlattices (e.g., alternating Si-Ge or InAs-InP) containing hundreds of repeat units (*14*–*16*). To achieve this, the precursors are alternated for the growth of each layer. The formation of 1D superlattices by this same time-dependent variation of precursor concentration is out of reach for present colloidal growth techniques. The largest number of alternating layers produced so far is three, and yet the sequence of purifications required in that instance was already taxing to implement (*17*).

Cation exchange provides a facile method for systematically varying the proportion of two chemical compositions within a single nanocrystal. We have previously shown that cation exchange can be used to fully (and reversibly) convert CdSe, CdS, and CdTe nanocrystals to the corresponding Ag-chalcogenide nanocrystal by a complete replacement reaction of the Cd^{2+} cations for Ag^{+} cations (*18*). The resultant material is the Ag-anion analog of the starting material (i.e., Ag_2Se, Ag_2S, and Ag_2Te). The size and shape of the nanocrystal are preserved when the nanocrystal has minimum dimensions greater than 4 nm (*18*). The high mobility of cations in the CdS(Se,Te) lattice suggests that partial cation exchange may lead to interesting patterns of segregated domains of Ag chalcogenide within a Cd-chalcogenide nanorod. This led us to investigate the possibility of converting a previously formed nanorod of a single chemical composition into a striped pattern by a single-step partial chemical transformation. In the case explored here, a linear arrangement of regularly spaced Ag_2S dots contained within a CdS rod forms spontaneously at ~36% cation exchange. The near-infrared (NIR) band gap of the Ag_2S dots is embedded within the larger gap of the CdS, creating a type I heterostructure with interesting optical properties.

Studies of partial cation exchange for 4.8–by–64-nm CdS to CdS-Ag_2S nanorods are shown in transmission electron microscopy (TEM) images in Fig. 1. In these experiments, the initial CdS nanorods (Fig. 1A) were exceptionally smooth and the rod diameter was tightly controlled (SD = 10%), whereas the length varied between 30 and 100 nm. The CdS colloidal nanorods were added to a solution of toluene, $AgNO_3$, and methanol at –66°C in air (*19*). The concentration of $AgNO_3$ was a controlled fraction of the concentration of Cd^{2+} ions present in the starting material. In the presence of excess Ag^{+}, the rods are completely converted to Ag_2S (*18*). However, when the Ag^{+} ions are limited to yield approximately 36% exchange, the resulting nanorods displayed a periodic pattern of light- and dark-contrast regions (Fig. 1, B and C). The average spacing between the dark regions is 13.8 nm, with a standard deviation of 28% (Fig. 1C, inset). The spacing between periodic segments can be controlled by the diameter of the initial CdS rod (fig. S1).

Examination of these regions shows that the light- and dark-contrast regions are CdS and Ag_2S, respectively. Energy-dispersive x-ray spectroscopy (EDS) indicates that the striped rods alternate between Cd-S– and Ag-S–rich regions (Fig. 2A) (*20*). Powder x-ray diffraction (XRD) data confirms the presence of wurtzite CdS and monoclinic acanthite Ag_2S (Fig. 2B) (*21*). Peaks appearing in the original CdS rods can be indexed to wurtzite CdS [Joint Committee on Powder Diffraction Standards (JCPDS) #41-1049], and those in the fully exchanged rods can be indexed to acanthite (JCPDS #14-0072). Peaks visible in the striped rods can be attributed

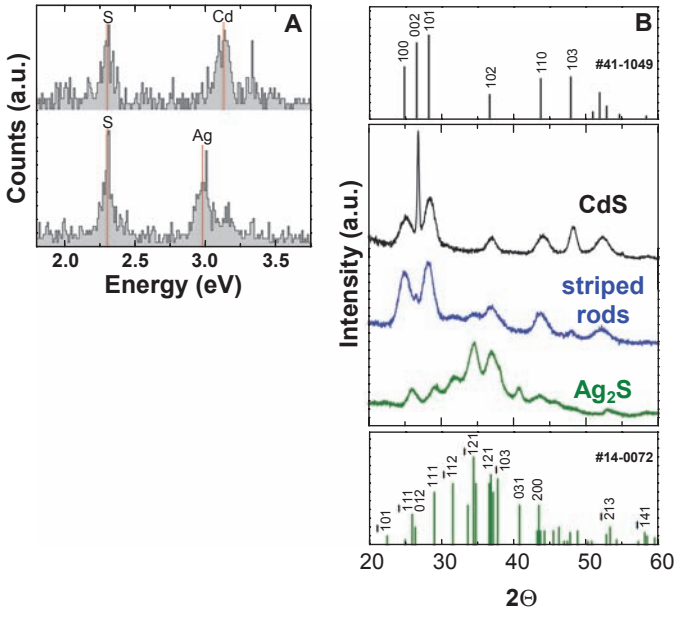

Fig. 2. Characterization of CdS-Ag_2S heterostructures. (**A**) EDS spectra of the striped rods at the (top) light- and (bottom) dark-contrast regions, corresponding to Cd-S– and Ag-S–rich regions, respectively. a.u., arbitrary units. (**B**) XRD spectra of CdS rods (black line), striped rods (blue line), and fully exchanged Ag_2S rods (green line). Spectra from the striped rods show new peaks corresponding to Ag_2S and a modified (002) peak, indicating interruption of the CdS lattice along the rod axis.

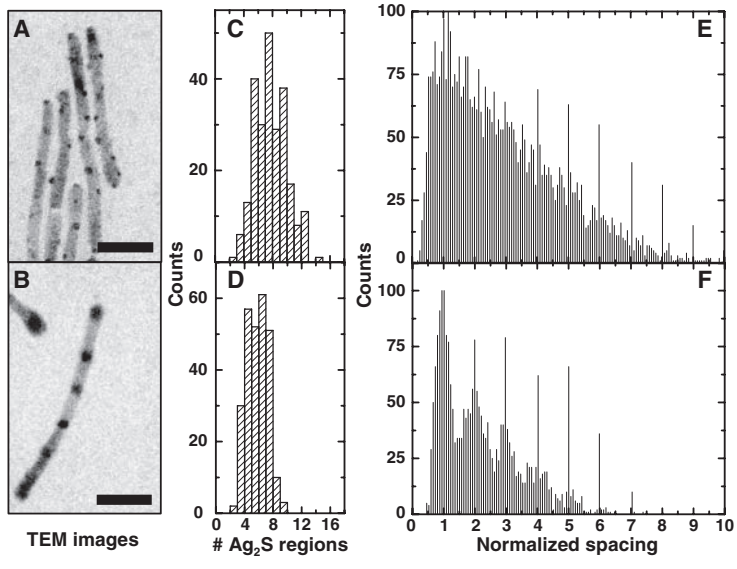

Fig. 3. Effects of increasing $AgNO_3$ concentration. (**A** and **B**) TEM images. (A) Low concentration (Ag^{+}/Cd^{2+} ~0.2). (B) Intermediate concentration that produced the nanorod superlattices (Ag^{+}/Cd^{2+} ~0.9). Scale bar (A and B), 20 nm. (**C** and **D**) Histograms of the number of Ag_2S regions per rod. (C) Low and (D) intermediate concentration. More than 250 nanorods were examined for each histogram. (**E** and **F**) Pair-distribution histograms for Ag_2S regions on individual CdS-Ag_2S nanorods. (E) Low and (F) intermediate concentration. Intrarod distances between each Ag_2S region, measured for 200 nanorods in each of the sample sets shown in (A) and (B). Spacings were normalized by the number of Ag_2S regions and the length of the rod. Low concentration (E) shows no correlation beyond the nearest-neighbor spacing. Intermediate concentration (F) shows a periodicity, which extends over several nearest neighbors.

purely to a combination of these two phases. No Ag peaks are present. Furthermore, a simulation of the XRD pattern for a mixture of Ag_2S and CdS crystalline domains with dimensions matching those of the sample agrees qualitatively with the experimental patterns, in terms of the relative intensities of Ag_2S peaks to CdS peaks, supporting the extent of the conversion observed in TEM images (fig. S2). In our experimental XRD patterns, the CdS (002) peak is broader and weaker for the striped rods than for the initial CdS sample. This indicates a decreased CdS crystallite size along <001> [the growth axis of the rods (*22*)] after the partial ion exchange. Debye-Scherrer analysis of peak widths for several striped-rod samples indicates that the CdS grain size along the axis has decreased from >30 nm to 12 to 16 nm for the striped rods. The decrease in grain size along this direction is attributed to the interruption of the {001} planes by the Ag_2S material, because the shorter length is consistent with the average spacing in this striped-rod sample. TEM images show that the Ag_2S regions, which have a broad range of separations at low concentrations (Fig. 3A), become increasingly ordered at slightly higher concentrations (Figs. 1, B and C, and 3B). The change in the number and periodicity (spacing) of the Ag_2S regions suggest a systematic organization as the volume fraction of Ag_2S increases (Fig. 3, C to F). Intrarod Ag_2S spacings were correlated through a pair-distribution function in which the distances between each Ag_2S region and all other Ag_2S regions on a rod were measured. The organization of the Ag_2S regions into superlattices is seen in the periodicity of the histogram (Fig. 3F), extending over several nearest-neighbor distances. In the superlattices, the Ag_2S regions are spaced evenly along the rod, whereas no periodicity is seen for the lower Ag^+ concentration (Fig. 3E).

The mechanism by which the initial arrangement of randomly distributed small islands of Ag_2S evolves into a periodic, 1D pattern is of particular interest. Because there exists a positive CdS-Ag_2S interface formation energy (~1.68 eV per Cd-Ag-S elementary interface unit, from our ab initio calculations), it is energetically favorable to merge small Ag_2S islands into larger Ag_2S segments. The fast diffusion of cations leads to a situation where Ostwald ripening between the initially formed islands of Ag_2S can occur, so that larger islands grow at the expense of nearby smaller ones. Diffusion of the cations is allowed because both Ag^+ and Cd^{2+} are considered fast diffusers (*23*–*25*). Also, Ag chalcogenides exhibit superionic conductivity in their high-temperature phases (*25*). A critical juncture occurs when the regions of Ag_2S grow to the point where they span the diameter of the rod. At this point, further Ostwald ripening is kinetically prohibited, because an atom-by-atom exchange of Ag^+ among segments will not reduce the total interfacial area. This leads to Ag_2S segments of nearly equal size (fig. S3). The rod is in a metastable state; i.e., the complete joining of two Ag_2S regions is always a lower-energy configuration, but one that cannot readily be accessed by simple atomic-exchange events.

A second factor that promotes the regular spacing of the stripe pattern is the elastic repulsion between two Ag_2S segments because of the strain in the intervening CdS region. A model for the coherent atomic connection between the two materials is shown in Fig. 4A (*26*). To match the basal lattice constant for CdS (4.3 Å), the Ag_2S body-centered–cubic lattice in the plane of interface has to expand by 4% in one direction and contract by 15% along the perpendicular direction. There is a repulsive elastic force between segments of like material because of the resulting strain fields. Results from valence force field (VFF) modeling (*27*) show that the elastic energy stored in the rod increases markedly as two Ag_2S segments approach each other (Fig. 4B). Bond strain in the z direction (axial) is responsible for the repulsive elastic interaction (Fig. 4C). CdS atoms are pushed away from the closest Ag_2S segment, forming convex-shaped atomic layers. For two Ag_2S segments approaching each other, the z displacements in the CdS are in opposite directions, leading to an interaction term between the fields that gives higher strain energy at smaller separations (*28*). The model is consistent with the experimental finding that increasing the rod diameter increases the spacing between segments (fig. S1). Similar effects of spontaneous ordering of quantum dots in two dimensions produced by MBE growth have been explained with corresponding arguments [e.g., (*3*)]. However, the 1D geometry explored here imposes a stronger constraint on ripening processes, leading to an especially robust path to stable, regularly spaced quantum dots within a rod.

The importance of strain in attaining the superlattice pattern can be illustrated by examining

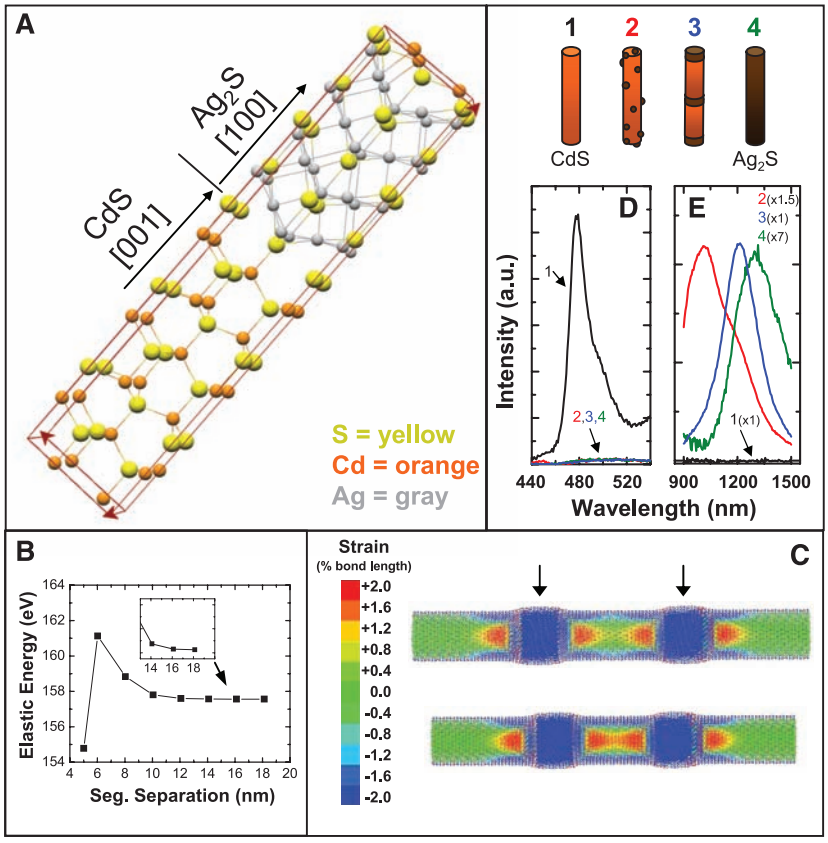

Fig. 4. Theoretical modeling and experimental optical characterization. (**A**) Cubic-cutout representation of cells used for ab initio energy calculations. A distorted monoclinic Ag_2S (100) plane connects with the wurtzite CdS (001) plane. (**B**) Elastic energy of the rod as a function of segment separation (center-to-center). (**C**) Z-axis strain for the case of two mismatched segments at a center-to-center separation distance of 14.1 nm (top) and 12.1 nm (bottom). The elastic interaction between segments is greatly reduced for separations >12.1 nm. Arrows show the placement of mismatched segments. The CdS rods used for VFF calculations (B and C) were 4.8 nm in diameter, with two 4.8–by–4.0-nm lattice-mismatched segments. Effective elastic constants for the mismatched segments were from ab initio calculations for monoclinic Ag_2S. (**D**) Visible and (**E**) NIR PL spectra at λ = 400- and 550-nm excitation, respectively. Coupling between the CdS and Ag_2S is evident by the complete quenching of the visible PL (D) in the heterostructures. The shift in NIR PL (E) is due to quantum confinement of the Ag_2S.

similar studies of metal ions reacting with semiconductor nanocrystals. Mokari *et al.* and Saunders *et al.* have created interesting metal-semiconductor nanocrystal heterostructures by reducing Au^{3+} ions onto InAs quantum dots (*29*) and CdS/Se nanorods (*30*, *31*). Because Au^{3+} has a much greater electron affinity than Ag^{+}, reduction of the ion takes place rather than an exchange reaction. The positive interfacial energy between the two materials drives a phase segregation, similar to our Ag_2S-CdS system, leading to Ostwald ripening. However, epitaxial strain does not play a major role in the Au growth, and these heterostructures continue to ripen into single-metal domains, either at the tip of the rod (CdS/Se), or inside the quantum dot (InAs). In contrast, the epitaxial relationship between the two phases in the Ag_2S-CdS superlattice structures results in strain fields from the lattice mismatch, which cause like segments to repel each other, preventing further ripening.

The resulting striped rods display properties expected of a type I array of Ag_2S quantum dots separated by confining regions of CdS, in agreement with our ab initio calculations of the band structure. The visible CdS photoluminescence (PL) is quenched, indicating coupling between materials at the heterojunction (*32*), and NIR PL from the Ag_2S segments is observed (Fig. 4, D and E). The band gap of the Ag_2S segments depends on their size, matching the bulk value (*33*) for fully converted nanorods and shifting to higher energy in smaller dots because of quantum confinement (Fig. 4E). In the present configuration, the Ag_2S quantum dots are only very weakly coupled to each other, because the CdS segments are large. Such structures are of interest for colloidal quantum-dot solar cells, where the sparse density of electronic states within a dot may lead to multiple-exciton generation (*34*). The formation of nanorod superlattices through partial cation exchange can also be applied to other pairs of semiconductors, yielding a broader class of quantum-confined structures. Cation-exchange reactions have already been reported in HgS, Ag_2S, SnS_2, CdS, ZnS, Cu_2S, Bi_2S_3, and Sb_2S_3 (*35*–*37*). Two-component combinations of these compounds can produce materials with functional properties ranging from type I (e.g., ZnS-Ag_2S) and type II (e.g., Cu_2S-CdS) band alignments to thermoelectric-power junctions (e.g., CdS-Bi_2S_3).

References and Notes

1. S. Guha, A. Madhukar, K. C. Rajikumar, *Appl. Phys. Lett.* **57**, 2110 (1990).
2. M. S. Miller *et al.*, *J. Appl. Phys.* **80**, 3360 (1996).
3. V. A. Shchukin, D. Bimberg, *Rev. Mod. Phys.* **71**, 1125 (1999).
4. R. Notzel, *Semicond. Sci. Technol.* **11**, 1365 (1996).
5. M. Law, J. Goldberger, P. D. Yang, *Annu. Rev. Mater. Res.* **34**, 83 (2004).
6. M. Bruchez Jr., M. Moronne, P. Gin, S. Weiss, A. P. Alivisatos, *Science* **281**, 2013 (1998).
7. W. C. W. Chan, S. Nie, *Science* **281**, 2016 (1998).
8. M. Achermann *et al.*, *Nature* **429**, 642 (2004).
9. I. Gur, N. A. Fromer, M. L. Geier, A. P. Alivisatos, *Science* **310**, 462 (2005).
10. D. Y. Li, Y. Wu, R. Fan, P. D. Yang, A. Majumdar, *Appl. Phys. Lett.* **83**, 3186 (2003).
11. M. S. Dresselhaus *et al.*, *Phys. Solid State* **41**, 679 (1999).
12. G. Kästner, U. Gösele, *Philos. Mag.* **84**, 3803 (2004).
13. E. Ertekin, P. A. Greaney, D. C. Chrzan, T. D. Sands, *J. Appl. Phys.* **97**, 114325 (2005).
14. Y. Y. Wu, R. Fan, P. D. Yang, *Nano Lett.* **2**, 83 (2002).
15. M. S. Gudiksen, L. J. Lauhon, J. Wang, D. C. Smith, C. M. Lieber, *Nature* **415**, 617 (2002).
16. M. T. Bjork *et al.*, *Nano Lett.* **2**, 87 (2002).
17. D. J. Milliron *et al.*, *Nature* **430**, 190 (2004).
18. D. H. Son, S. M. Hughes, Y. Yin, A. P. Alivisatos, *Science* **306**, 1009 (2004).
19. Materials and methods are available as supporting material on *Science* Online.
20. A minority of segments are Ag-rich with little or no S, probably due to the decomposition of Ag-S compounds by the electron beam (*38*). This beam damage also distorted the phase and prevented accurate images from being acquired with high-resolution TEM.
21. For these experiments, TEM images show that the original CdS rods were 5.3 by 50 nm, and the striped rods made from these had 5.3–by–11-nm CdS grains.
22. X. Peng *et al.*, *Nature* **404**, 59 (2000).
23. T. D. Dzhafarov, M. Serin, D. Oren, B. Sungu, M. S. Sadigov, *J. Phys. D Appl. Phys.* **32**, L5 (1999).
24. H. H. Woodbury, *Phys. Rev.* **134**, A492 (1964).
25. M. Kobayashi, *Solid State Ionics* **39**, 121 (1990).
26. In both common polymorphs of Ag_2S (cubic and monoclinic), the anion sublattice assumes a body-centered–cubic structure with only slight distortions in the monoclinic phase (*39*). Several epitaxial relationships were considered, and the epitaxial connection with minimal lattice distortion to the (001) CdS face is the body-centered–cubic (110) face [monoclinic (100) face].
27. A. J. Williamson, L. W. Wang, A. Zunger, *Phys. Rev. B* **62**, 12963 (2000).
28. When the segments are very close to each other, however, the elastic energy is actually lowered. With only three atomic layers separating the segments (leftmost point in Fig. 4B), the number of distorted layers in the *z* direction is small, which results in a smaller repulsive interaction. Additionally, the interaction of the radial distortions from the two segments is cooperative (unlike the *z*-direction distortions), because they pull the atoms in the same direction. The overall result is a lowering of the elastic energy.
29. T. Mokari, A. Aharoni, I. Popov, U. Banin, *Angew. Chem. Int. Ed.* **45**, 8001 (2006).
30. T. Mokari, E. Rothenberg, I. Popov, R. Costi, U. Banin, *Science* **304**, 1787 (2004).
31. A. E. Saunders, I. Popov, U. Banin, *J. Phys. Chem. B* **110**, 25421 (2006).
32. D. Battaglia, B. Blackman, X. Peng, *J. Am. Chem. Soc.* **127**, 10889 (2005).
33. P. Junod, H. Hediger, B. Kilchor, J. Wullschleger, *Philos. Mag.* **36**, 941 (1977).
34. V. I. Klimov, *J. Phys. Chem. B* **110**, 16827 (2006).
35. A. Mews, A. Eychmuller, M. Giersig, D. Schooss, H. Weller, *J. Phys. Chem.* **98**, 934 (1994).
36. C. D. Lokhande, V. V. Bhad, S. S. Dhumure, *J. Phys. D Appl. Phys.* **25**, 315 (1992).
37. L. Dloczik, R. Koenenkamp, *J. Solid State Electrochem.* **8**, 142 (2004).
38. L. Motte, J. Urban, *J. Phys. Chem. B* **109**, 21499 (2005).
39. H. Schmalzried, *Prog. Solid State Chem.* **13**, 119 (1980).

40. This work was supported by the U.S. Department of Energy under contract no. DE-AC02-05CH11231. We thank C. Nelson, C. Kisielowski, the National Center for Electron Microscopy at Lawrence Berkeley National Laboratory. We also thank D. Talapin, T. Teague, and D.-H. Son. R.D.R. thanks the Lawrence Berkeley National Laboratory for the Lawrence Postdoctoral Fellowship.

Supporting Online Material

www.sciencemag.org/cgi/content/full/317/5836/355/DC1
Materials and Methods
SOM Text
Figs. S1 to S3
References

15 March 2007; accepted 29 May 2007
10.1126/science.1142593

A Late Triassic Dinosauromorph Assemblage from New Mexico and the Rise of Dinosaurs

Randall B. Irmis,[1]* Sterling J. Nesbitt,[2,3]* Kevin Padian,[1] Nathan D. Smith,[4,5] Alan H. Turner,[3] Daniel Woody,[6] Alex Downs[7]

It has generally been thought that the first dinosaurs quickly replaced more archaic Late Triassic faunas, either by outcompeting them or when the more archaic faunas suddenly became extinct. Fossils from the Hayden Quarry, in the Upper Triassic Chinle Formation of New Mexico, and an analysis of other regional Upper Triassic assemblages instead imply that the transition was gradual. Some dinosaur relatives preserved in this Chinle assemblage belong to groups previously known only from the Middle and lowermost Upper Triassic outside North America. Thus, the transition may have extended for 15 to 20 million years and was probably diachronous at different paleolatitudes.

Dinosaurs originated in the Late Triassic Period (*1*, *2*) (Carnian-Norian stages, about 230 to 200 million years ago), when they replaced faunas dominated by a variety of basal archosaurs and other amniotes (*3*, *4*). Archosaurs are divided into two primary lineages: the Pseudosuchia, which include phytosaurs, aetosaurs, "rauisuchians," and crocodylomorphs, and the Ornithodira, which include pterosaurs, basal dinosauromorphs such as